Hydrodynamic disassembly and expansion of electron-beam-heated warm dense copper

J. E. Coleman, H. E. Morris, M. S. Jakulewicz, H. L. Andrews, and M. E. Briggs
Los Alamos National Laboratory, Los Alamos, New Mexico 87545, USA

(Received 23 April 2018; published 8 October 2018)

Cu foils, 200 μm in thickness, were heated in two stages by a ~100-ns-long monoenergetic electron bunch at 19.8 MeV and a current of 1.7 kA (8.5×10^{14} e^-) in a 2-mm-spot to $T_e \sim 1$ eV. After 45 ns of isochoric heating, the pressure in the foil builds up to >20 GPa (200 kbar), it begins to hydrodynamically disassemble, and a velocity spread is measured. Near the end of the electron pulse, the 1550 nm probe is cut off or absorbed. Photonic Doppler velocimetry measurements were made to quantify the expansion velocity, hydrodynamic disassembly time, and pressure of the foil prior to cutoff. Measurements indicate foil motion begins the instant electrons pass through the foil and continues until the particle velocity approaches the ambient sound velocity of Cu and the bulk density exceeds the critical density of the probe. Once the density of the plasma drops below the critical threshold and begins reflecting again, an expansion velocity of the classical plasma is also measured, similar to the point-source solution.

DOI: 10.1103/PhysRevE.98.043201

I. INTRODUCTION

Pressure and velocity are essential measurements for the equation of state (EOS) in the warm-dense-matter (WDM) regime. WDM is a low-temperature plasma at nearly solid density covering the parameter space of $0.1 < T_e$ (eV) <10 and $10^{22} < n_e$ (cm^{-3}) $<10^{24}$ for most metals. WDM is typically strongly coupled ($\Gamma \sim 1$) and degenerate due to the Fermi energy >1 eV compared to lower-density classical plasmas [1–3]. The EOS and shock Hugoniot for Cu have been investigated in detail for the past 30 years [4–9]; however, those measurements were done using gas gun shock compression techniques, and as of yet no plasma properties have been measured.

In the plasma physics and shock physics communities, velocity measurements are typically made on shock-compressed materials and gases over a wide range of pressures. These pressures range from MPa for plate impact experiments on noble gases [10] to TPa for shock compression of MgO [11]. These velocities are typically measured using two techniques: a velocity interferometer system for any reflector (VISAR) [12,13] and photonic Doppler velocimetry (PDV) [14].

VISAR measurements have traditionally been fielded on laser shock compression experiments to measure shock velocity (u_s) versus particle velocity (u_p) along the shock Hugoniot. 85 eV blackbody radiation was used to shock-compress Be to 360 GPa [15]. 250–300 J of green laser light was used to provide spherical and planar shocks to 0.3–1-mm-thick Si and recorded velocities up to 0.8 km/s [16]. 500 J of laser energy was used to dynamically compress 20–50 μm of MgO and evaluate two crossover points in the Hugoniot at 350 and 650 GPa ($u_s \sim 15$ and 18 km/s) [11].

PDV has been used to measure initial shocks and flyer plates in gas gun experiments [10,14,17]. Reference [10] measured shocked Ar from plate impact at pressures of 1.4–6.9 MPa. Reference [14] evaluated initial shock arrival in explosively driven metal. Reference [17] measured ~1 km/s velocities on the surface of 1-mm-thick ferrite impacted by a 250 μm Mylar flyer. PDV has also been used to measure shock velocities of 250-nm-thick Ti from laser ablated Si [18] and the polymorphic transition of shock compressed Sn up to 44 GPa [19].

As mentioned in a previous review [20], WDM has been produced and characterized by several approaches, with the largest contribution coming from the laser community. Several authors (only a small subset is referenced here) have produced isochoric heating with sub-ps pulses at peak amplitudes in 0.1–100-μm-thick targets [21–24]. In most of these experiments, there is a laser prepulse (or a slight contrast) that deposits energy in the foil and generates a preplasma. This preplasma sheath accelerates electrons to a range of energies that in turn provide the heating. The lasers range from a low intensity of 10^{17} W/cm^2 [21] producing 20 keV class electrons to 2×10^{20} W/cm^2 [24], which is estimated to produce electrons with a large range of relativistic energies. These approaches rely heavily on two-dimensional (2D) particle-in-cell simulations and collisional Monte Carlo codes to predict both the electron energy distribution and the energy deposition into the target. A stacked bremsstrahlung spectrometer in combination with Monte Carlo simulations estimated the electron energy distribution ranging from 10^{14} electrons at the low-energy end of 1 MeV dropping exponentially below 10^{11} electrons at 14 MeV from laser impact on 600-μm-thick Al-Cu sandwiched targets at an intensity of 8×10^{19} W/cm^2 [23]. Similar estimates were made by Ref. [24] indicating just under 10^{12} electrons with energy >4 MeV dropping exponentially to 10^7 electrons at energies of 100 MeV for laser intensities of 2×10^{20} W/cm^2. Although these experiments claim an isochoric heating process, simulations by Ref. [24] indicate the prepulse causes premature energy deposition by lower energy electrons and expansion before the peak of the pulse.

WDM produced directly by particle beam impact has been investigated with ions through several approaches, but only recently with monochromatic relativistic electrons [20,25]. GSI has used GeV-class uranium ions to heat W, Au, and Pb [26,27]. The NDCX-I and NDCX-II facilities have heated

Au and Sn targets [28–33]. Lasers have been used to accelerate protons and Al^+ ions to heat C and Au samples [34–36]. Reference [35] measured expansion speeds of 6.7 and 7.5 μm/ns (km/s) for C and Au over a 5 ns window heated by laser accelerated ~140-MeV Al^+ ions. Reference [26] measured a 2.6 km/s expansion velocity for a Pb foil heated with 83.3 GeV U^{73+} ions. In addition, the Pb target pressure and displacement were indirectly measured ~1 μs after heating by measuring the displacement history on volume constraining sapphire plates [37]. These particle-beam-driven approaches [20,25,26,35] have been used to measure the expansion of the subsequent plasma with optical imaging techniques, but not the target itself. To date there has been no direct measurement of the target dynamics for particle-beam-driven, collisional, isochoric heating of a solid target: hydrodynamic disassembly time, pressure, and target velocity.

Recently, we began investigating two-stage heating with a monochromatic 20 MeV, 1.7 kA bunch of electrons [20,25]. The physics of experiments producing relativistic electron plasmas are much different from direct heating with monochromatic relativistic electrons for several reasons: how the energy is initially deposited, the number of particles providing the heating, heating time scales, and the energy distribution of the particles. We have demonstrated production of a large homogeneous volume (3×10^{-4} cm^3) and mass (2.8 mg) of warm dense Ti and Cu and measured $T_e > 1.25$ eV and $n_e = 3 \times 10^{17}$ cm^{-3} in the expanded less degenerate state. To help confirm this slower heating technique, relative to isochoric heating techniques performed with short pulse lasers and laser shock-compression experiments, we have fielded a single collimated PDV probe to provide our first EOS measurement. This provides a measurement of the foil velocity, hydrodynamic disassembly time, and hydroexpansion of the warm dense copper (WDCu), and we obtain a possible estimate of the lifetime of the warm dense phase.

II. ISOCHORIC HEATING AND HYDRODYNAMIC DISASSEMBLY

In previous reviews, the heating and expansion process for electron-beam-driven Ti and Cu was explained [20,25]. Briefly, we are performing an identical two-stage heating technique. The first stage, which is considered isochoric, is early in the electron pulse $t < t_{\text{hydro}}$. $t_{\text{hydro}} = \Delta z/2C_o$ is the hydrodynamic disassembly time of a thin foil, where C_o is the shock velocity at infinitesimally small particle velocity or the sound velocity at ambient pressure, and Δz is the foil thickness. C_o is 3.93 km/s (μm/ns) for Cu, so t_{hydro} for a 200-μm-thick Cu foil is 25.4 ns. From the measurements below it is estimated that the isochoric heating process lasts until 45 ns for 200-μm-thick Cu. Prior to this time, >50% of the ρ_o remains constant. Simulations indicate a similar performance as will be explained below.

Recent PDV measurements help validate the previously observed adiabatic expansion images and analytic calculations [20,25]. In addition, we are actively measuring the expansion velocity, foil displacement, and pressure in the foils before disassembly. The foils are securely fastened into a rigid target paddle assembly, which can be translated vertically and provides optical access both upstream and downstream of the foil. A single collimated PDV probe with a working distance of 14 in. (>30 cm) was installed on a reentrant tube on the vacuum section (Fig. 1) to bring the probe spot within 500 μm at this working distance. Recall the electron beam spot is 2 mm. The probe was oriented at 20° relative to the foil surface to avoid interference with the electrons transmitted through the foil. The probe orientation is shown with a 90-ns time gated image of the visible light emission from a Cu plume for illustration. Since the probe is at 20°, it is measuring $v_z\cos(20°)$ because the surface has a roughness ~2 μm. Due to the probe wavelength $\gg$ than the surface roughness of Cu, we are able to measure nonspecular backscattering from the rough surface unambiguously [38,39]. The probe provides a measurement over a large range of velocities with ns temporal resolution and 10 μs of time history. However, this measurement is only done along the probe axis and therefore does not completely capture the spherical plume expansion measured through imaging in [20,25]. The measurement is very sensitive to alignment and often requires a pilot shot on the foil for precise alignment to within 250 μm of the center of the electron beam spot.

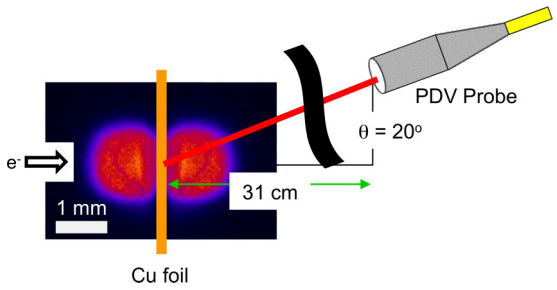

FIG. 1. Experimental setup displaying an electron-beam-heated Cu foil (not to scale), an expanding plume (false color), and a PDV probe oriented 20° off normal of the foil face on the downstream side. The expanded plume, shown for reference, is the visible light emitted from the plasma over 90 ns, 20 ns after beam energy deposition begins. Scales are shown for reference.

Figure 2(a) provides an example shot in which we measure the voltage response or beat wave from the PDV probe of an electron-heated 200-μm-thick Cu foil. Figure 2(a) shows a 150 ns snap shot while the electron beam is depositing energy compared to the 10-μs window shown in the inset. At $t = 0$ ns we measure a rapid rise in the signal to 250 mV for close to 5 ns. This is the initial elastic motion of the foil due to electrons hitting the surface, depositing energy, and beginning the melt process, which requires 0.13 J. The electrons are depositing energy at a rate of <0.2 J/ns. After this point, $t > 10$ ns, the signal amplitude is reduced by 50%, has a +50 mV bias offset, and the beat wave begins to dampen out from ±100 mV at 10 ns to ±50 mV for $t > 25$ ns. The noise level of this signal is ~25 mV so the S/N is close to 10 and begins to decrease once the foil disassembles.

Examining the corresponding spectrogram in Fig. 2(b), we see there is a strong velocity band from 0 to 25 ns with a slope (acceleration) ~35 mm/(μs)^2. The velocity spectrogram is calculated from the beat frequency, $f_{\text{beat}} : v(t) = cf_{\text{beat}}/2f_o = 1/2f_{\text{beat}}\lambda_o$, where c is the speed of light, and f_o and λ_o are the probe reference frequency and wavelength, 1550 nm. The beat frequency is calculated from the Doppler-

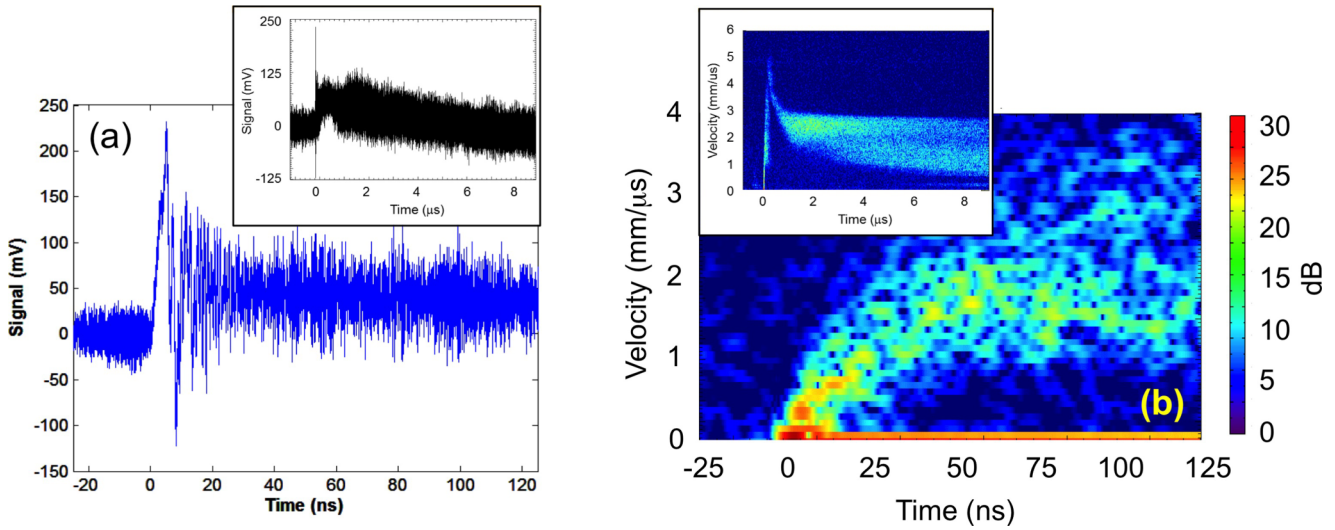

FIG. 2. (a) Zoomed-in version of the measured voltage response on the PDV probe with electrons incident on the foil at $t = 0$; the full 10-μs record is shown in the inset. (b) The calculated velocity spectrogram for this 150 ns window is shown indicating the hydromotion of the foil; the full 10-μs spectrogram is shown in the inset. All data for shot number 25901.

shifted frequency f_D measured with respect to the reference probe where $f_{\text{beat}} = f_D - f_o$.

Once the $\langle v \rangle$ in the spectrogram reaches 1.6 mm/μs (km/s) [$t = 45$ ns in Figs. 2(b) and 4(a)], the slope in the velocity is reduced, the signal is reduced to <20 dB, and a ~15% velocity spread is measured for close to 80 ns. This is an indication of hydrodynamic disassembly of the foil. Reference [7] indicates that plastic deformation of Cu begins at particle velocities $u_p > 0.75$ km/s (mm/μs), and Refs. [8,17] indicate the measurement of a slow elastic precursor wave prior to the shock breakout (or the plastic wave). It is our belief that we are observing an elastic wave from 0 to 10 ns, after which the foil begins to accelerate at a fairly constant rate up to 45 ns. Then the material begins to disassemble, a plume forms, and a ~15% velocity spread is measured. A velocity spread is being measured because the probe is penetrating a Cu plume, and a range of fast and slow particles (ejecta, lower density plasma) are crossing the probe path from 45 to 125 ns. The minimum estimated particle size we can measure is $>\lambda_o/2$ based on Mie scattering theory [40,41]. Based on these measurements and observations from hydrosimulations below, once the foil begins to disassemble we are transitioning into WDM. These measurements and hydrosimulations represent a possible advantage of producing and diagnosing WDM with this slower heating technique.

To help better understand the dynamics of this heating process and compare the measurements to the tabulated EOS, the LASNEX [42] 2D Lagrangian radiation-hydrodynamics code was used to model the expansion of the electron-beam-heated Cu. These simulations were performed using an axisymmetric geometry and solve the Navier-Stokes equations with artificial viscosity and electron thermal conduction, plus multigroup radiation diffusion. The energy was deposited using a particle beam source; electron beam collisional stopping power and ionization cross sections were used to accurately represent the collisional heating process. Since Cu was the target material used, we used the EOS table SESAME 3336 [9,43]. The LASNEX model was used to estimate the electron temperature, density, average ionization, motion of the foil surface, and pressure within the foil. From these simulations, we were able to make a direct comparison of the foil motion and pressure to the PDV measurements. To accurately model the experiment, the proper current pulse, energy deposition rate, and energy density distribution must be used. Two-dimensional edge effects are not observed for this material, but they are easily resolved with axial zone sizes <1 μm at $t = 0$ and adapting in size to 1.1 μm at 32 ns when the calculated pressure begins to release, as indicated below.

The time-resolved electron temperature, density, and average ionization at 50 ns intervals are shown in Fig. 3. These are calculated along the axis within the first radial zone, which is 17 μm. The initial solid density of Cu is 7.8×10^{22} cm^{-3} so the peak n_e increases >3× in 50 ns due to the higher ionization states during the isochoric heating process [Fig. 3(a)]. The pressure builds up in the material during the heating process and then it releases, WDCu forms, and expansion begins. The electron density decreases to $1.3n_o$ at 100 ns and continues to drop as the material expands but remains in the warm dense phase for >200 ns. The electron density does not drop below the cutoff density for the PDV probe until we are 500-μm from the target center at 150 ns.

In the first 50 ns, while the heating is isochoric, the calculated temperature ranges from 0.5 eV at the edge to 0.65 eV near the center [Fig. 3(b)]. After this point, WDCu exists and we continue to dump energy into the expanding plasma, heating it to just under 0.95 eV at the center at 100 ns. Later the calculated T_e drops back to 0.6 eV 500-μm from the center at 150 ns and >0.5 eV 600-μm from target center at 200 ns. Heating to these temperatures, Cu^{3+} ions may exist near the target center and begin to relax to average ionization levels above Cu^{+} for >200 ns [Fig. 3(c)]. These ionization states at 150 and 200 ns agree well with spectroscopy measurements made during this time frame with a thinner foil in [25].

We have examined the initial hydroexpansion of the 200-μm-thick foils for three consecutive shots during this heating process and see <10% variation in the leading edge

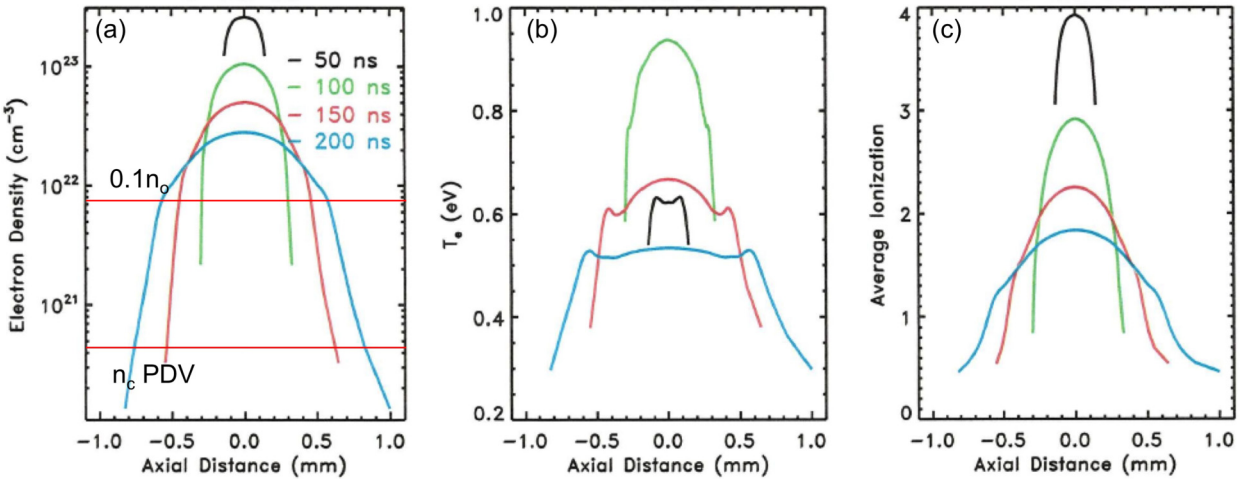

FIG. 3. LASNEX calculation of the axial electron (a) density, (b) temperature, and (c) ionization state for a 200-μm Cu foil at 50 ns intervals from 50 to 200 ns. 10% solid density is indicated in addition to the critical density for PDV in (a).

velocity. The leading edge velocity is defined as the maximum measured velocity in the spectrogram where the minimum signal is 12 ± 2 dB. For illustration we only show the results from shot 25901 in comparison with the LASNEX simulation in Fig. 4. First we examine the mean velocity from the spectrogram in Fig. 2(b) and we compare it to the leading edge to get the maximum particle motion [Fig. 4(a)]. The average velocity profile is calculated by selecting a region-of-interest from the spectrogram in Fig. 2(b) within a signal threshold of 10 dB. The mean velocity indicates a linear ramp instantly and increases to $\langle v \rangle = 1.6$ mm/μs at 45 ns, where it begins to flatten out. Examining the fastest particle movement from the leading edge of the spectrogram, we see a faster acceleration $\sim$50 mm/(μs)^2 for the first 50–60 ns. The acceleration of the leading edge also slows down, and just after 100 ns we measure peak velocities near 4 mm/μs. The calculated velocity from LASNEX has a similar velocity slope with the leading edge until $\sim$70 ns, after which the slope is reduced but extends above the measurement. Keep in mind this calculation neglects the cutoff density effect, which limits the experimental probe in measuring the peak velocity after warm dense matter is formed.

By simply integrating the measured velocity v we can calculate the foil displacement at the edge, $\delta z = z_o + \int v(t)dt$. The average expanded location of the foil face is indicated in Fig. 4(b). The initial movement is slow, and then the expansion rate tends to increase at a steady rate; the average expansion is $<$200 μm. The leading edge indicates a maximum particle displacement $>$300 μm away from the original surface, and this tends to agree fairly well with the EOS calculation in LASNEX. Keep in mind that this is the estimated foil movement at the edge from a velocity measurement and is not necessarily representative of movement of the whole foil volume. In addition, there may be small errors in the displacement due to the probe being 20° off normal [39]. During the initial expansion, prior to disassembly, we can calculate the pressure in the elastic limit: $P_E(t) = 1/2 C_o v(t) \rho(t)$, where $\rho(t)$ is the calculated density derived from the measured expanded volume $V(t) = V_o + 2A\delta z$ and the heated mass of material interrogated by the probe. This is an approximation because the volume is expanding spherically, but the probe can only measure the expansion along the probe axis [38,39]. A is the initial heated area of the foil. As stated above, once the average velocity reaches 1.6 ± 0.2 mm/μs, nearly 45 ns after energy deposition begins [Figs. 2(b) and 4(a)], the average pressure exceeds 20 GPa (200 kbar) and then the material begins to release or hydrodynamically disassemble [Fig. 4(c)]. We see a similar trend with the leading edge, as reduced

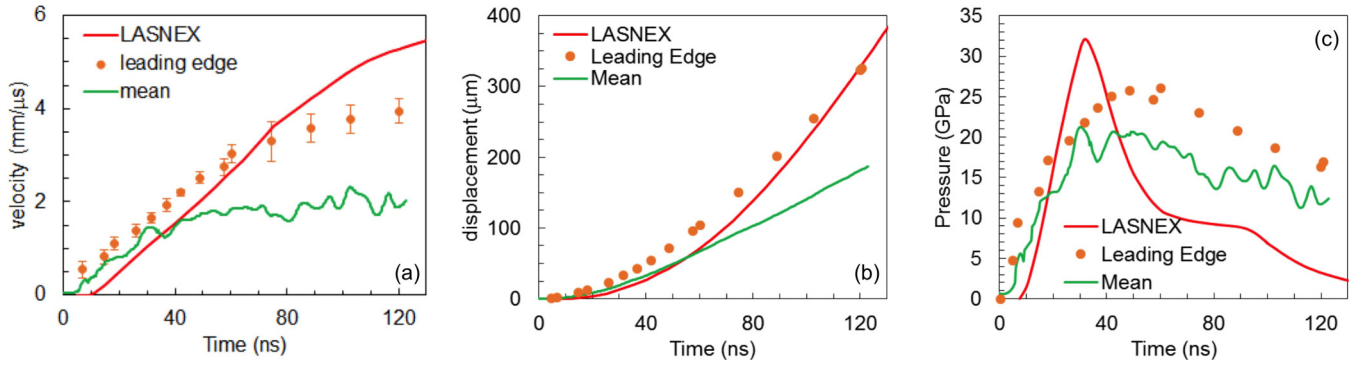

FIG. 4. Red, LASNEX calculation, Orange dots: experimentally measured values from the leading edge of the spectrogram in Fig. 2(b), Green: mean of the experimentally measured spectrogram. (a) particle velocity; (b) foil displacement at the edge and; (c) elastic pressure, from a 200-μm-thick copper foil for shot number 25901 vs. EOS pressure at the center of the foil.

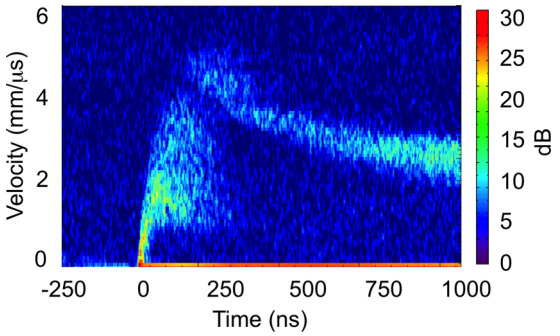

FIG. 5. An expanded velocity spectrogram out to 1 μs from the same foil hydromotion from Fig. 2(b) indicating the temporal velocity spread and cutoff time for shot number 25901.

acceleration tends to coincide with a pressure release at a slightly later time compared with the average case; the peak pressure we infer from measurements is near 25 GPa. We calculate a slightly faster rise in pressure with LASNEX and a peak pressure of 32 GPa, 20% higher than the experiment. This pressure is calculated at the center 800 nm axial zone and the center 17 μm radial zone of the foil; the calculated pressure averaged along the entire axis at disassembly is 24 GPa. Each of these is fairly close to the solid-density Fermi pressure of 33 GPa [44]. In addition, this pressure is close to the tabulated shock Hugoniot data at 5 km/s [45], which is the maximum velocity we measure at 160 ns (Fig. 5). The electrons are uniformly heating the foil through collisions with Cu atoms, stripping electrons from the atom, and increasing temperature and pressure throughout the volume. This is isochoric heating until the material disassembles and releases pressure, since $>50\%$ of ρ_o remains constant until this point. We do not believe there is a shock based on these observations and the agreement with the EOS table SESAME 3336 [9,43]. Pressure evaluation with the Hugoniot relations is at least $3\times$ higher.

Despite the foil beginning to hydrodynamically disassemble at 45 ns, which is also where we begin to generate WDM, we still continue to measure particle velocities well beyond the 100 ns pulse length of the electron beam (Fig. 5). We measure a velocity range of 1–4 mm/μs over a 45–250 ns time window. We reach a peak velocity of 4 mm/μs near 120 ns, and above this point the signal is cut off and there are no longer any particles in the probe path with a velocity greater than this until 160 ns. The cutoff density for 1550 nm is 4.6×10^{20} cm^{-3}, which is $\sim 200\times$ below solid density Cu (7.8×10^{22} cm^{-3}). We believe that during this 120–160 ns time window the probe is being absorbed or strongly attenuated by the dense material in its path, then it proceeds to expand and cool off. Higher velocities may exist, as calculated by LASNEX, at $t < 160$ ns from the higher temperature dense plasma, but they are not measured due to absorption of the 1550 nm light. Near 160 ns we measure a peak velocity of 5 mm/μs, and beyond that point we measure the expansion of the recombining classical plasma.

III. ADIABATIC EXPANSION

As indicated from the LASNEX calculations (Fig. 3) and measurements in Fig. 5, 120 ns after disassembly begins ($t = 160$ ns), the density, 500-μm from the original foil edge ($z = 600$ μm), drops below the cutoff and the plasma begins cooling; at this point we begin measuring the slowing down velocity of the adiabatically expanding plasma. The initial velocity band we measure at 160 ns is 4.4–5.0 mm/μs. Examining Figs. 2(b) and 5 more closely, we can see that the particle velocity reduces down to a range of 1.9–3.0 mm/μs at 1 μs and continues to slow down to 0.9–2.8 mm/μs at 5 μs and 0.57–2.7 mm/μs at 9 μs. Although we see a significant slowing down feature, we also have particles maintaining $v > 2.7$ mm/μs for close to 10 μs, clearly indicating we have a range of velocities due to a plume expanding close to ~ 1 cm along the direction of the probe path. Performing a fit to the slowest velocities over the 1–7 μs band in Fig. 2(b), we obtain $v(t) \sim t^{-0.76}$, which is a slightly slower deceleration than we observed from images in Ref. [25] and expected from the point-source solution [46–48].

IV. CONCLUSION

We have fielded a PDV probe and demonstrated time-resolved velocity measurements on a Cu foil heated purely by electrons in a two-stage process. The voltage response on the PDV probe indicates a short ~ 10 ns elastic precursor and $t_{\mathrm{hydro}} = 45$ ns for a 200-μm-thick foil. These measurements indicate the release at $\langle v \rangle$ and $\langle P \rangle$ of 1.6 mm/μs (km/s) and 21 GPa. The pressure is calculated assuming an elastic expansion since we are isochorically heating during this first stage and there is no presence of a shock. The measured peak pressure agrees reasonably well with LASNEX simulations and the calculated Fermi pressure. After the material is released and WDM is formed, a range of velocities is measured due to the probe being intersected by an expanding plume.

A peak expansion velocity of 4 mm/μs (km/s) is measured prior to the probe being cut off or absorbed. The velocity distributions are extremely repeatable with identical foils and precise alignment of the probe. There are visible trends of reduced t_{hydro}, foil deflection, and pressure for thinner foils, but the relationship is not linear. We also measure a slow-down velocity spectrum that agrees fairly well with the observed adiabatic expansion from previous plume images and analytic approximations. These measurements confirm the onset of hydrodynamic disassembly for an electron-beam-heated foil, the generation of a warm dense plasma, and the existence of WDM >200 ns.

ACKNOWLEDGMENTS

This work was supported by the National Nuclear Security Administration of the U.S. Department of Energy under Contract No. DE-AC52-06NA25396. We would like to thank C. A. Bolme, W. T. Buttler, J. Danielson, C. A. Ekdahl, J. P. Harding, R. Hixson, S. D. McGrane, and G. Rodriguez for their technical discussions. We would like to take the opportunity to thank Don Roeder and Sharon Dominguez for their manufacturing and design support. We would like to thank the operators, technicians, and engineers Doug Aikin, Robbie Brooks, Jules Carson, Josh Esquibel, Raul Gonzalez, Kris Peterson, Melissa Reed, Tony Sanchez, Sam Snider, Rudy Valdez, and Travis Weaver for their continued support.

[1] *Committee on High Energy Density Plasma Physics, National Research Council, Frontiers in High Energy Density Physics: The X-Games of Contemporary Science* (The National Academies Press, Washington, DC, 2003).

[2] R. W. Lee, S. J. Moon, H. K. Chung, W. Rozmus, H. A. Baldis, G. Gregori, R. C. Cauble, O. L. Landen, J. S. Wark, A. Ng, and S. J. Rose, J. Opt. Soc. Am. B **20**, 770 (2003).

[3] A. B. Zylstra, J. A. Frenje, P. E. Grabowski, C. K. Li, G. W. Collins, P. Fitzsimmons, S. Glenzer, F. Graziani, S. B. Hansen, S. X. Hu, M. G. Johnson, P. Keiter, H. Reynolds, J. R. Rygg, F. H. Séguin, and R. D. Petrasso, Phys. Rev. Lett. **114**, 215002 (2015).

[4] A. C. Mitchell and W. J. Nellis, J. Appl. Phys. **52**, 3363 (1981).

[5] A. C. Mitchell, W. J. Nellis, J. A. Moriarty, R. A. Heinle, N. C. Holmes, R. E. Tipton, and G. W. Repp, J. Appl. Phys. **69**, 2981 (1991).

[6] W. J. Nellis, A. C. Mitchell, and D. A. Young, J. Appl. Phys. **93**, 304 (2003).

[7] E. M. Bringa, J. U. Cazamias, P. Erhart, J. Stölken, N. Tanushev, B. D. Wirth, R. E. Rudd, and M. J. Caturla, J. Appl. Phys. **96**, 3793 (2004).

[8] R. Chau, J. Stölken, P. Asoka-Kumar, M. Kumar, and N. C. Holmes, J. Appl. Phys. **107**, 023506 (2010).

[9] J. H. Peterson, K. G. Honnell, C. Greeff, J. D. Johnson, J. Boettger, and S. Crockett, AIP Conf. Proc. **1426**, 763 (2012).

[10] D. M. Dattelbaum, P. M. Goodwin, D. B. Garcia, R. L. Gustavsen, J. M. Lang, T. D. Aslam, S. A. Sheffield, L. L. Gibson, and J. S. Morris, AIP Conf. Proc. **1793**, 090004 (2017).

[11] K. Miyanishi, Y. Tange, N. Ozaki, T. Kimura, T. Sano, Y. Sakawa, T. Tsuchiya, and R. Kodama, Phys. Rev. E **92**, 023103 (2015).

[12] L. M. Barker and R. E. Hollenbach, J. Appl. Phys. **43**, 4669 (1972).

[13] P. M. Celliers, D. K. Bradley, G. W. Collins, D. G. Hicks, T. R. Boehly, and W. J. Armstrong, Rev. Sci. Instrum. **75**, 4916 (2004).

[14] O. T. Strand, D. R. Goosman, C. Martinez, T. L. Whitworth, and W. W. Kuhlow, Rev. Sci. Instrum. **77**, 083108 (2006).

[15] P. M. Celliers, D. J. Erskine, C. M. Sorce, D. G. Braun, O. L. Landen, and G. W. Collins, Rev. Sci. Instrum. **81**, 035101 (2010).

[16] R. F. Smith, C. A. Bolme, D. J. Erskine, P. M. Celliers, S. Ali, J. H. Eggert, S. L. Brygoo, B. D. Hammel, J. Wang, and G. W. Collins, J. Appl. Phys. **114**, 133504 (2013).

[17] S. Liu, D. Wang, T. Li, G. Chen, Z. Li, and Q. Peng, Rev. Sci. Instrum. **82**, 023103 (2011).

[18] A. R. Valenzuela, G. Rodriguez, S. A. Clarke, and K. A. Thomas, Rev. Sci. Instrum. **78**, 013101 (2007).

[19] C. Chauvin, Z. Bouchkour, F. Sinatti, and J. Petit, AIP Conf. Proc. **1793**, 060013 (2017).

[20] J. E. Coleman and J. Colgan, Phys. Rev. E **96**, 013208 (2017).

[21] K. Eidmann, U. Andiel, F. Pisani, P. Hakel, R. C. Mancini, G. C. Junkel-Vives, J. Abdallah, and K. Witte, J. Quant. Spectrosc. Radiat. Transf. **81**, 133 (2003).

[22] F. Perez, L. Gremillet, M. Koenig, S. D. Baton, P. Audebert, M. Chahid, C. Rousseaux, M. Drouin, E. Lefebvre, T. Vinci, J. Rassuchine, T. Cowan, S. A. Gaillard, K. A. Flippo, and R. Shepherd, Phys. Rev. Lett. **104**, 085001 (2010).

[23] F. Perez, S. D. Baton, M. Koenig, C. D. Chen, D. Hey, M. H. Key, S. Le Pape, T. Ma, H. S. McLean, A. G. MacPhee, P. K. Patel, Y. Ping, F. N. Beg, D. P. Higginson, C. W. Murphy, H. Sawada, B. Westover, T. Yabuuchi, K. U. Akli, E. Giraldez, M. Hoppe, Jr., C. Shearer, R. B. Stephens, L. Gremillet, E. Lefebvre, R. R. Freeman, G. E. Kemp, A. G. Krygier, L. D. Van Woerkom, R. Fedosejevs, R. H. Friesen, Y. Y. Tsui, and D. Turnbull, Phys. Plasmas **17**, 113106 (2010).

[24] M. Schollmeier, A. B. Sefkow, M. Geissel, A. V. Arefiev, K. A. Flippo, S. A. Gaillard, R. P. Johnson, M. W. Kimmel, D. T. Offermann, P. K. Rambo, J. Schwarz, and T. Shimada, Phys. Plasmas **22**, 043116 (2015).

[25] J. E. Coleman and J. Colgan, Phys. Plasmas **24**, 083302 (2017).

[26] P. A. Ni, F. M. Bieniosek, M. Leitner, B. G. Logan, R. M. More, P. K. Roy, D. H. H. Hoffmann, D. Fernengel, A. Hug, J. Menzel, S. Udrea, N. A. Tahir, D. Varentsov, H. Wahl, M. Kulish, D. N. Nikolaev, V. Ya., A. Fertman, A. A. Golubev, B. Yu. Sharkov, and J. J. Barnard, Overview of warm-dense-matter experiments with intense heavy ion beams at GSI-Darmstadt, in *Proceedings of the Particle Accelerator Conference, Albuquerque, NM* (IEEE, New York, 2007), p. 2038.

[27] P. A. Ni, M. I. Kulish, V. Mintsev, D. N. Nikolaev, V. YA. Ternovoi, D. H. H. Hoffmann, S. Udrea, A. Hug, N. A. Tahir, and D. Varentsov, Laser Part. Beams **26**, 583 (2008).

[28] J. E. Coleman, Ph.D. Thesis, University of California, Berkeley, 2008.

[29] F. M. Bieniosek, J. J. Barnard, A. Friedman, E. Henestroza, J. Y. Jung, M. A. Leitner, S. Lidia, B. G. Logan, R. M. More, P. A. Ni, P. K. Roy, P. A. Seidl, and W. L. Waldron, J. Phys.: Conf. Ser. **244**, 032028 (2010).

[30] P. A. Ni, F. M. Bieniosek, E. Henestroza, and S. M. Lidia, Nucl. Instrum. Methods Phys. Res., Sect. A **733**, 12 (2014).

[31] P. A. Seidl, A. Persaud, W. L. Waldron, J. J. Barnard, R. C. Davidson, A. Friedman, E. P. Gilson, W. G. Greenway, D. P. Grote, I. D. Kaganovich, S. M. Lidia, M. Stettler, J. H. Takakuwa, and T. Schenkel, Nucl. Instrum. Methods Phys. Res., Sect. A **800**, 98 (2015).

[32] P. A. Seidl, J. J. Barnard, R. C. Davidson, A. Friedman, E. P. Gilson, D. Grote, Q. Ji, I. D. Kaganovich, A. Persaud, W. L. Waldron, and T. Schenkel, J. Phys.: Conf. Ser. **717**, 012079 (2016).

[33] P. A. Seidl (private communication).

[34] A. Pelka, G. Gregori, D. O. Gericke, J. Vorberger, S. H. Glenzer, M. M. Günther, K. Harres, R. Heathcote, A. L. Kritcher, N. L. Kugland, B. Li, M. Makita, J. Mithen, D. Neely, C. Niemann, A. Otten, D. Riley, G. Schaumann, M. Schollmeier, An. Tauschwitz, and M. Roth, Phys. Rev. Lett. **105**, 265701 (2010).

[35] W. Bang, B. J. Albright, P. A. Bradley, D. C. Gautier, S. Palaniyappan, E. L. Vold, M. A. Santiago Cordoba, C. E. Hamilton, and J. C. Fernández, Sci. Rep. **5**, 14318 (2015).

[36] W. Bang, B. J. Albright, P. A. Bradley, E. L. Vold, J. C. Boettger, and J. C. Fernandez, Phys. Rev. E **92**, 063101 (2015).

[37] M. Kulish, A. Fertman, A. Golubev, A. Tauschwitz, and V. Turtikov, Rev. Sci. Instrum. **72**, 2294 (2001).

[38] D. H. Dolan, AIP Conf. Proc. **1195**, 589 (2009).

[39] M. E. Briggs, E. A. Moro, M. A. Shinas, S. McGrane, and D. Knierim, J. Phys.: Conf. Ser. **500**, 142005 (2014).

[40] S. K. Monfared, W. T. Buttler, D. K. Frayer, M. Grover, B. M. LaLone, G. D. Stevens, J. B. Stone, W. D. Turley, and M. M. Schauer, J. Appl. Phys. **117**, 223105 (2015).

[41] M. M. Schauer, W. T. Buttler, D. K. Frayer, M. Grover, B. M. LaLone, S. K. Monfared, D. S. Sorenson, and G. D. Stevens, J. Dyn. Behav. Mater. **3**, 217 (2017).

[42] G. B. Zimmerman and W. L. Kruer, Comments on Plasma Physics and Controlled Fusion **2**, 51 (1975).

[43] The SESAME EOS library is a binary, tabular compendium of equations of state for numerous materials and is maintained and disseminated by Group T-1 at the Los Alamos National Laboratory (email: sesame@lanl.gov).

[44] R. P. Drake, *High-Energy-Density Physics: Foundation of Inertial Fusion and Experimental Astrophysics*, 2nd ed. (Springer, New York, 2017).

[45] *Los Alamos Shock Hugoniot Data*, edited by S. P. Marsh (University of California Press, Berkeley, 1979).

[46] H. A. Bethe, K. Fuchs, J. O. Hirschfelder, J. L. Magee, R. E. Peierls, and J. von Neumann, BLAST WAVE, Los Alamos Report LA-2000, Chap. 2 (1947).

[47] G. I. Taylor, Proc. R. Soc. A **201**, 159 (1950).

[48] G. I. Taylor, Proc. R. Soc. A **201**, 175 (1950).